Optik - International Journal for Light and Electron Optics 247 (2021) 167976

Contents lists available at ScienceDirect

Optik

journal homepage: www.elsevier.com/locate/ijleo

Spinel oxide incorporated photoanode for better power conversion efficiency in dye-sensitized solar cells

Umesh Fegade [a,*], Yu-Chen Lin [b], Chia-Ching Lin [b], Inamuddin [c], Ren-Jang Wu [b,*], Badriah Alshahrani [d], Thamraa Alshahrani [d,*], Amir Al-Ahmed [e], Firoz Khan [e], Mohd Taukeer Khan [f], Nafis Ahmad [g]

[a] Department of Chemistry, Bhusawal Arts, Science and P. O. Nahata Commerce College, Bhusawal, MH 425201 India
[b] Department of Applied Chemistry, Providence University, Shalu, Taichung 433, Taiwan
[c] Department of Applied Chemistry, Zakir Husain College of Engineering and Technology, Faculty of Engineering and Technology, Aligarh Muslim University, Aligarh 202 002, India
[d] Department of Physics, College of Science, Princess Nourah bint Abdulrahman University, Riyadh 11671, Saudi Arabia
[e] Interdisciplinary Research Center for Renewable Energy and Power Systems (IRC-REPS), King Fahd University of Petroleum & Minerals, Dhahran 31261, Saudi Arabia
[f] Department of Physics, Faculty of Science, Islamic University of Madinah, Prince Naifbin Abdulaziz, Al Jamiah, Madinah 42351, Saudi Arabia
[g] Department of Physics, College of Science, King Khalid University, P.O. Box 9004, Abha 61413, Saudi Arabia

ARTICLE INFO

Keywords:
Dye-sensitized solar cell
Photoanode
$ZnMn_2O_4$
Power conversion efficiency

ABSTRACT

In this study, $ZnMn_2O_4$ (ZMO) nanoparticles were synthesized and mixed with the commercial TiO_2 to prepare composite photoanode. Dye sensitized solar cells (DSSC) device was fabricated and highest power conversion efficiency of 5.09% was obtained for the cell with 0.1 wt% of ZMO in the photoanode, while in similar condition the device with pure TiO_2 photoanode showed power conversion efficiency of 4.124%. This improvement in the power conversion efficiency of the composite photoanode based cell was attributed to the presence of critical amount of ZMO which synergistically improve the light absorption, charge transport properties prevented charge recombination, eventually it improved open-circuit voltage (V_{oc}) and short-circuit current (I_{sc}).

1. Introduction

Energy demand is increasing exponentially consequently environment pollution is also increasing. To address the issues of energy demand, several renewable energy resources are explored, such as, solar, wind, geothermal etc. Among these resources solar energy is abundant and have different mature harvesting technologies [1,2]. Solar cell based solar energy harvesting technologies are convenient way to produce electricity. Among the different solar cells, silicon (Si) based systems are dominating the market. However, processing of Si to its pure crystalline form is costly and energy intense process [3]. That is why several low-cost thin film solar cell technologies are getting considerable attention.

During the 90s, dye-sensitized solar cells (DSSCs) were one of the promising member of this family [1,4], when Michael Grätzel reported a DSSC with titanium dioxide (TiO_2) as photoanode and used ruthenium based metal organic complex as photosensitizer (dye), iodide ions (I^-/I^{3-}) based electrolyte and platinum based counter electrode. This cell showed a power conversion efficiency (PCE)

* Corresponding authors.
E-mail addresses: umeshfegade@gmail.com (U. Fegade), rjwu@pu.edu.tw (R.-J. Wu), thmalshahrani@pnu.edu.sa (T. Alshahrani).

https://doi.org/10.1016/j.ijleo.2021.167976
Received 18 June 2021; Received in revised form 23 August 2021; Accepted 12 September 2021
Available online 17 September 2021

of 7.1% which was much higher than any of the previously reported DSSCs [5–7]. The manufacturing cost of the DSSC is low, can also be fabricated on flexible substrate having high mechanical strength, can generate electricity under low illumination conditions and can come in different colors [5–7]. Modification of the conventional photoanode with other transition metal oxide nanoparticles is an effective approach to improve the performance of the DSSC. This modification can improve the light absorption, charge transport properties and suppress the recombination to improve the interfaces energy. However, at present DSSC technology is facing strong challenges with other thin film solar cell technologies to catch up the efficiency and stability. One of the main reasons of the inferior performance of DSSC is the charge carrier's recombination. The photo-electron generated from dye can pass into electrolyte and recombined with holes, such phenomenon also termed as dark current [8].

In DSSC, an improved photo-anode can play a crucial role to separate and transport the charges in more efficient manner which can eventually enhance the performance [7,8]. To do so, researchers have tried different approaches, like, modification of the morphologies of TiO_2 to nanoparticles, nanoroads, nanotube, mesoporous structure, nanosheets and even nanowires [8–12]. Similarly, by preparing composite photo-anode, doping of photo-anode with different metals and metal oxides, alternatively different types of dyes and electrolytes have also been investigated to improve the power conversion efficiency of DSSCs [1,6,7]. In a similar approach, Eguchi et al. [13] fabricated DSSC using Nb_2O_5-TiO_2 composite photoanode and this electrode based device showed better power conversion efficiency (PEC) compared to that of the pure TiO_2 based device. Feng et al. [14] used the tantalum(Ta)-doped TiO_2 nanowires as photoanode. The PEC of the Ta-doped TiO_2 photoanode based solar cell was found to be slightly higher (4.1%) than the pure TiO_2 photoanode based cell (4.06%). The short circuit current density (J_{sc}), open-circuit voltage (V_{oc}) and fill factors (FF) for these typical devices were: 7.5 mA, 900 mV, and 63% for Ta-doped TiO_2 photoanode; 8.1 mA, 750 mV, and 68% for un-doped TiO_2 photoanode. Duan [15] et al. used Sn-doped TiO_2 based photoanode and found a good PCE of 8.31%, which was significantly higher than the PEC of the pure TiO_2 (7.45%) based device. It was also observed that the PEC, J_{sc} and V_{oc} increased with increase amount of Sn content up to 0.50 mol. wt. %. However, further increase of Sn concentration negatively impacted the cell performance. At the higher concentration, agglomerated sites act as trapping spots for electron-hole recombination and reduced the transparency. This increased the charge recombination and reduced the photon absorption, resulted lower cell efficiency. Mehmood et al. enhanced the photovoltaic efficiency of DSSC through the impregnation of different metal oxides like, CeO_2 [8], ZnO [16] and Al_2O_3 [17]. Similarly, Younas et al. [18] used the tungsten oxide nanoparticles incorporated TiO_2 photoanode. It was observed that the modified surface structure of the photoanodes enhances the charge transport and charge recombination resistance which collectively improves the current density and efficiency of the cell [5–7]. The performance parameters of the photovoltaic cell are regulated by its cell parameters, photogenerated current density (J_{pH}), shunt resistance (R_{sh}), series resistance (R_s), diode ideality factor (n), reverse saturation current density (J_0). In DSSC, the reverse electron transfer causes the dark current which has a direct relationship with R_{sh}. Higher R_{sh} suppress the dark current and facilitate higher efficiency. The R_s is the total resistance of the cell i.e. transparent conducting oxide (TCO) layer, the resistance of the electron transfer at the TiO_2/dye/electrolyte interface and the resistance due to carrier transport at the counter electrode, respectively. Increasing R_s value decreases the J_{sc} and fill factor and eventually affects the efficiency [6].

On the other hand, spinel oxide zinc–manganese oxide ($ZnMn_2O_4$ (ZMO)) have been synthesized and studied for several

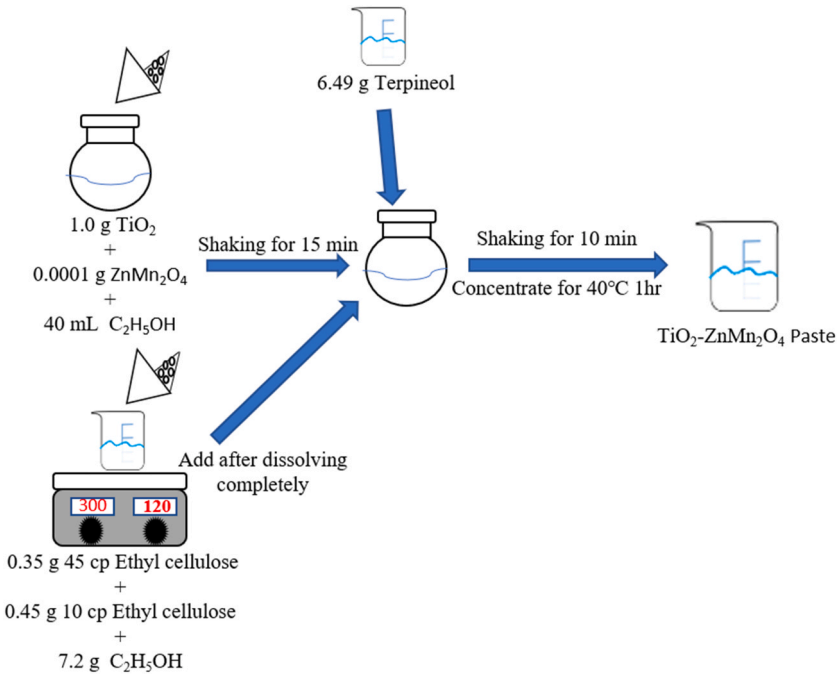

Fig. 1. Preparation of composite photoanode paste of TiO_2 (p25) and ZMO.

applications, such as, photo-catalysis [19], Li-ion batteries [20,21] etc. ZMO has found to have good absorption properties as well [22]. Moreover, both zinc and manganese are environment friendly and have low price tag [17]. Good optical absorption in the visible region and stability makes ZMO a promising component to engineer the optoelectric properties of the conventional TiO_2 based photoanode of the DSSC. This can facilities better charge separation and transportation, improve the J_{sc} and V_{oc} of the cell and ultimately better PCE. Therefore, in this work, ZMO nanoparticles were synthesized by modified co-precipitation method and characterized. The energy gap was calculated from UV-Vis response as 1.57 eV. Thereafter, composite photoanode pastes were prepared by mixing different wt% of ZMO and commercial TiO_2 (P25) nanoparticles to obtain better charge separation and transportation and eventually higher cell performance in a DSSC structure.

2. Materials and methods

2.1. Synthesis of ZMO

$ZnMn_2O_4$ (ZMO) was synthesized by modifying the previously reported method [23] using surfactant assisted co-precipitation technique followed by calcination. Typically, 2.72 g of $ZnCl_2$ and 6.04 g of $MnSO_4$ were taken in a Teflon beaker containing 1 g of sodium lauryl sulfate (SLS). 35 mL of 5 N NaOH solution was added slowly into this mixture at 50 °C followed by ultra-sonication for 2 h. After the precipitation, solids were collected by gravity centrifuge and repeatedly washed with deionized water (DIW) until the pH become neutral. Finally, solid precipitates were dried overnight in an air oven at 100 ℃ and grinded using a pestle and mortar and calcinated at 350 ℃ for 2 h. The process is shown schematically in Fig. 1.

2.2. Characterization of ZMO

The morphology and elemental property of the synthesized ZMO nanoparticles were characterized by high resolution transmission electron microscopy (HRTEM.JEOL JEM-2010). Structural property was investigated using XRD diffraction pattern (SHIMADZU). Absorption spectrum was acquired by using UV-Vis spectroscopy (T90 + UV/VIS Spectrometer and Varian Cary® 50). For comparison, commercial TiO_2 nanoparticles were also characterized. Amount of dye absorbed and amount of dye adsorption was calculated by Beer's law.

2.3. Composite photoanode paste preparation

A 0.05, 0.10, 0.20, 0.30, 0.50, 1.0 wt% of ZMO were added to required amount of commercial TiO_2 (P25) and mixed in absolute ethanol by ultrasonic oscillation for 20 min followed by grinding in a pestle and mortar to obtain 6 different photoanode compositions. In a beaker, 0.35 g of ethyl cellulose (viscosity of 45 cps (centipoise)) and 0.45 g of ethyl cellulose (viscosity of 10 cps) were taken and 7.2 g of absolute ethanol was added to dissolve the polymers. The mixture was stirred over a hotplate at 60 °C to accelerate the process. In a separate beaker TiO_2 (P25)+ZMO power was dispersed in 6.49 g of anhydrous terpineol and stirred for 10 min. Finally, viscous polymer solution was added to this second mixture and the stirring was continued for another 30 min to obtain uniform mixing. At the end, ethanol was evaporated in a rotatory evaporator at 40 °C to obtain a sticky photoanode paste.

2.4. DSSC fabrication

2.4.1. Working electrode fabrication

At first, FTOs were cleaned with detergent and rinsed with DIW followed by sonication for 15 min in ethanol and acetone, respectively. A machine was punching a circular hole with a diameter of 0.6 cm, and sticks the punched 3 M tape on the FTO on the conductive surface of the FTO conductive glass. The active surface area of DSSC was measured as 0.28 cm^2. Finally, the FTO dried in an air oven at 80 °C to obtain clean FTO substrates. Working electrode was prepared by coating the FTO with the photoanodes (pure and composites) using optimized tape coasting method followed by stepwise heating method, such as, 20 min at 200 °C, then temperature was raised to 500 °C and kept constant for another 1 h to bud all the organic moieties. The thickness of TiO_2 layer was measured by film thickness tester (Surfcorder ET200, Kosaka Laboratory Ltd.).

2.4.2. Preparation of dye

Weighed an appropriate amount of N719 dye powder, and used acetonitrile and tert-butanol as the solvent at a volume ratio of 1:1, then mixed well and the N719 dye solution at a concentration of 0.5 mM was obtained. The configuration of the dye solution is completely wrapped in aluminum foil and placed in a dark room to stock. Finally, the FTOs were cooled to room temperature and socked with N719 (0.5 mM) dye solution for 24 h. After dye soaking, all FTOs were rinsed gently with ethanol to remove any unanchored dye molecule.

2.4.3. Counter electrode

For the counter electrode, two small holes were drilled on the FTOs before cleaning. 0.015 M hexachloroplatinic acid ($H_2PtCl_6.6H_2O$) solution was drop casted on the cleaned FTOs and calcinated at 450 °C for 20 min and finally cooled to room temperature. To assemble the cell, a heat-sealable film (Surlyn) was used between anode and counter electrode and pressed for 15 min at 120 °C to fix and seal the electrodes. Prepared the PrMImI (1-Methyl-3-propylimidazolium iodide), I_2 (Iodine), LiI (Lithium iodide),

TBP (4-tert-Butylpyridine) and the solvent acetonitrile for the electrolyte fabrication. The electrolyte preparation way was to take 3.03 g of PrMImI and dissolve in 20 mL of acetonitrile, then added the 0.24 g of I_2, 1.35 g of TBP and 0.27 g of LiI in sequence, and stir for one day in the absence of light. Then, electrolyte was injected though the holes of the counter electrode using a syringe and finally these holes were sealed using 3 M tape to complete the device fabrication.

2.5. Solar cell characterization

J-V properties of the fabricated DSSC cells were studied by using SAN-EI 150W Simulator and Keithley2400. Incident photon-to-electron conversion efficiency (IPCE) was measured by using a 7ISW301 Triple Grating Monochromators. (7-STAR OPTICAL INSTRUMENTS CO. LTD., model 7-SCSpec).

3. Results and discussion

3.1. Morphological properties

TEM image of the commercial TiO_2 (P25) and synthesized ZMO are presented in Fig. 2. The TiO_2 nanoparticles were found to have spherical shape with particle size between 20 and 30 nm. The lattice size was observed to be around 0.35 nm for101 crystal planes (Fig. 2 a and b). On the other hand, ZMO nano particles were found to have slightly bigger particle size of around 40 nm, however, the lattice size was about 0.26 nm, which is consistent with ZMO (211) crystal plane (Fig. 2c and d). EDX analysis confirms the presence of zinc, manganese, and oxygen (Fig. 3).

3.2. Structural properties

Structural property of the synthesized ZMO nanoparticles was investigated using X-ray diffraction analysis. The spectrum is shown in Fig. 4. The P25 nanoparticles showed the characteristic peaks on crystal planes (101), (004), (200), (105), (211), and (204) at $2\theta = 25.28^\circ$, 37.80°, 48.05°, 53.89°, 55.06° and 62.69°, respectively which belong to the anatase form of P25 (TiO_2) [2,8]. For the ZMO, which has a Zn/Mn ratio of 1:2 (JCPDS Card No. 24–1133) showed the characteristic peaks on the crystal planes (112), (103), (211), (321), (224), (400). The diffraction peaks $2\theta = 29.3^\circ$, 33.03°, 36.3° in the reference literature corresponding to 59.01°, 60.77° and 65.1° belong to spinel ZMO [24]. The crystallite size has been calculated using X-ray diffraction data employing Scherrer's Eq. (1) [24,

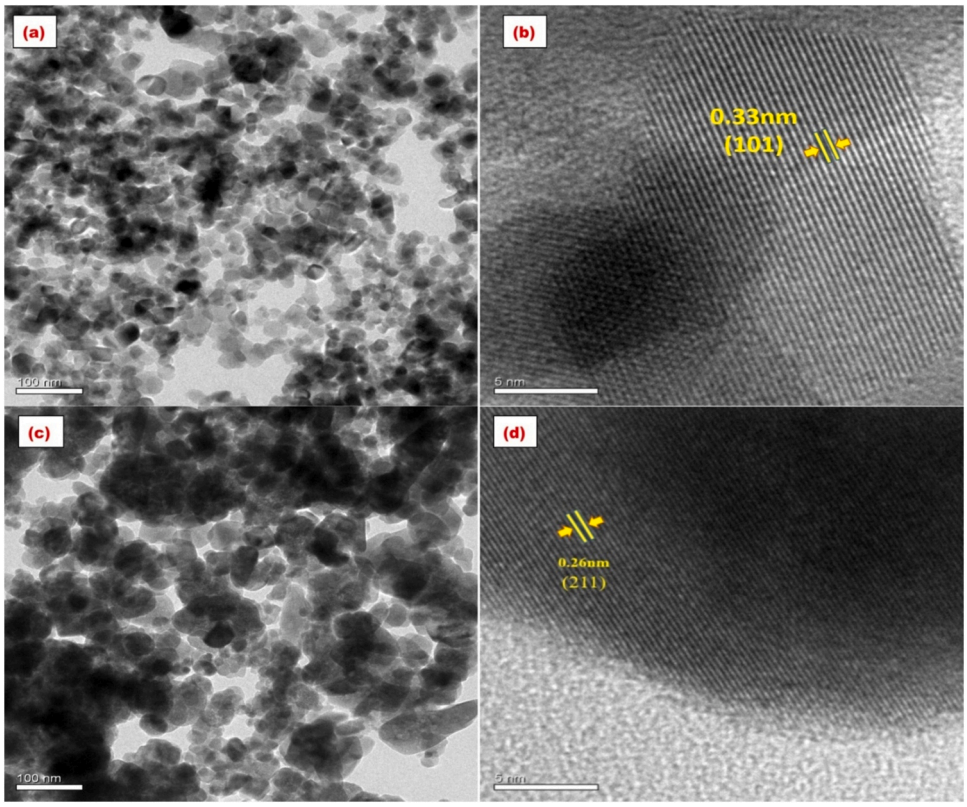

Fig. 2. TEM images of TiO_2 (p25) (a) 100 nm (b) 5 nm and ZMO (c) 100 nm (d) 5 nm.

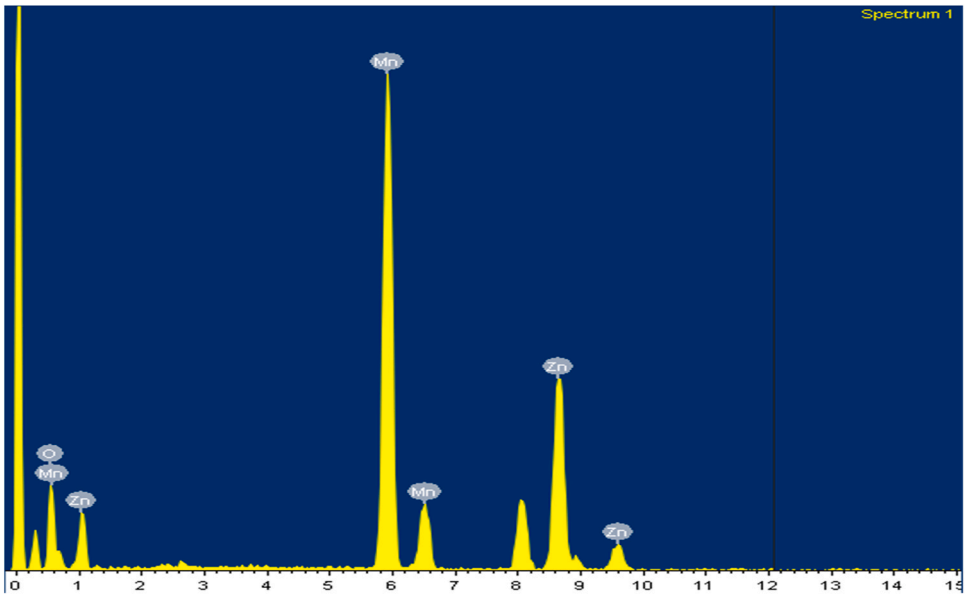

Fig. 3. EDX spectra of the ZMO.

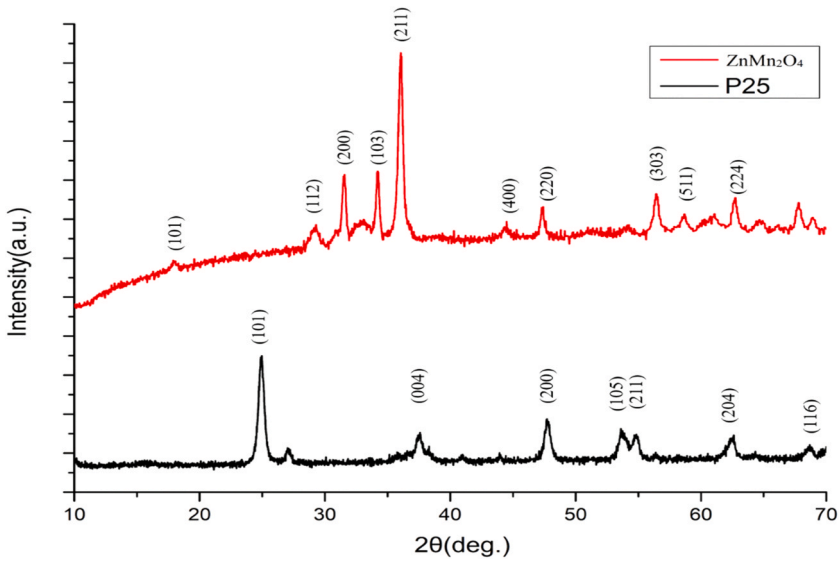

Fig. 4. XRD patterns of the obtained sample.

25].

$$D = \frac{0.94.\lambda}{\beta.Cos\theta} \tag{1}$$

where, D is crystallite size, λ is the used wavelength of X-ray, β is full width at half maximum (FWHM) of the diffraction peak (in radian), and θ is Bragg's angle. By calculating Scherrer equation, the average particle size of P25 and ZMO was found to be 26.19 and 25.99 nm, respectively.

3.3. Optical properties

Light absorption properties of the synthesized ZMO nanoparticles were studied by UV-Vis spectroscopy and compared with P25 results (Fig. 5). It was observed that the absorption of ZMO falls between 300 and 800 nm, whereas P25 showed the absorption region

between 200 and 400 nm. This suggest that the incorporation of ZMO can have synergistic effect to improve the light absorption properties of the composite photoanode, as observed in the previous reports [14,15]. The Tauc plot [26,27] was used to determine the band gap (E_g) using Eq. (2)

$$\alpha h\nu = A(h\nu - E_g)^n$$

where hυ = photon energy, α = absorption coefficient, A = constant, n = 2 for the direct bandgap materials. The Touc plot is displayed in Fig. 6. The bandgap was calculated as 1.57 eV, which was less than that of P25.

3.4. J-V and IPCE analysis

It was observed that the thickness of the photoanode has substantial influence on the performance of the cell performance [1,6, 28–30]. Therefore, photoanode with three different film thicknesses (20, 24 and 28 μm) were prepared using pure P25 and cell performance were analyzed (Table 1). Best performance was found for the cell with 24 μm thick TiO_2 (P25) photoanode film. Therefore, this film thickness was used for all other later experiments. The illuminated current density-voltage (*J-V*) characteristics of the DSSC of various doping of ZMO are shown in Fig. 7a. The performance parameters i.e., short circuit density (J_{sc}), open circuit voltage (V_{oc}), fill factor (FF), and conversion efficiency (η) are extracted from *J-V* curves and tabulated in the Table 2. It can be seen from Table 2 that the η of ZMO was very low (0.00024%). The best η of 5.09% (J_{sc} = 10.04 mAcm^{-2}, V_{oc} = 0.74 V and FF = 0.68) was obtained for the cell with 0.1 wt% ZMO. Higher photo current can be attributed to higher light absorption, reduction of electron transfers path length, and quick transportation of charge carriers. This increase in the current is one of the factors for improved IPCE as shown in Fig. 7b. However, the photon-to-electron conversion was nearly 5% higher for the 0.1 wt% ZMO doped photoanode based cell, which showed the highest photon-to-electron conversion rate of 40.7%. Therefore, it was concluded that the addition of ZMO with a smaller band gap improved the photon capture efficiency of the photoelectrode. All cells showed good V_{oc} and FF, which could be assigned to rapid transportation of charges and decrease in the recombination (Fig. 8). However, a slight reduction of cell performance was observed at lower and higher concentration of ZMO from the optimum level (0.1 wt%). At higher concentration there was agglomeration and light loss due to direct absorption by ZMO, which led to the poor charge collection and lower efficiency of the DSSCs. Similar observation was also reported in other work [8,31,32]. At lower concentration, it can be attributed to the lower points of contacts between P25 and ZMO, which hindered the charge movement.

3.5. PV cell parameter analysis

The performance parameters of the photovoltaic cell are regulated by photovoltaic (PV) cell parameters (Photogenerated current density (J_{pH}), shunt resistance (R_{sh}), series resistance (R_s), diode ideality factor (n) and reverse saturation current density (J_0)) [33,34]. The J_{pH} represents the equivalent current due to charge generation in the absorbing layer. A higher value of J_{pH} results for the higher short circuit current density, a higher conversion efficiency of the DSSC. The shunt resistance arises due the leakage current. It should be higher for a good DSSC. R_s is the total resistance of DSSC, which includes the resistance of the current collect, anode and cathode layers, electrolyte, and the absorbing layer. For the higher value of R_s, the FF value is reduced, which severely reduced the performance of the DSSC. n and J_0 represent the recombination occurring in the cell. For the higher value of n, the V_{oc} increased, however, it reduced

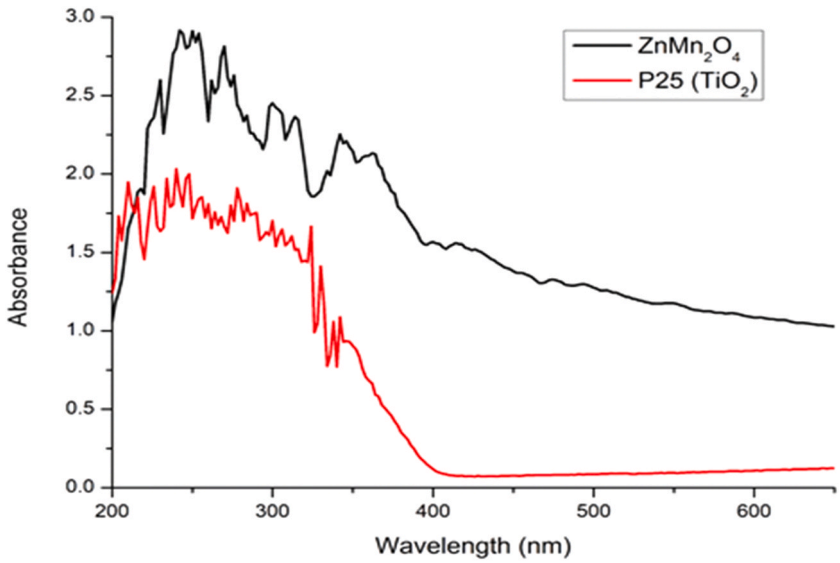

Fig. 5. UV-Vis absorption diagram of different materials.

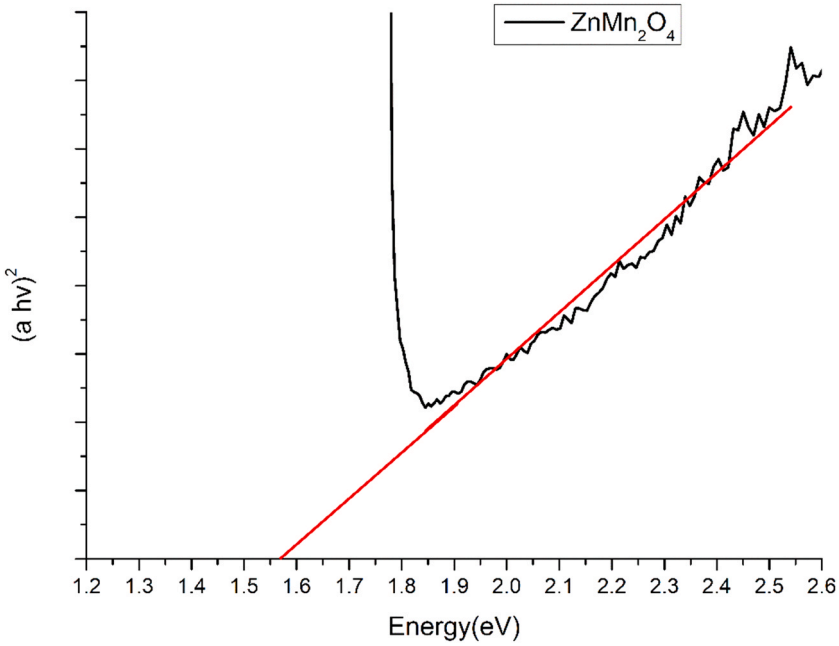

Fig. 6. Band gap diagram of ZMO.

Table 1
Comparison of titanium dioxide P25 electrode under different film thickness.

Film thin (μm)	V_{oc} (V)	J_{sc} ($mAcm^{-2}$)	FF	η (%)
20 μm	0.72	8.44	0.66	4.06
24 μm	0.71	8.58	0.68	**4.12**
28 μm	0.75	7.75	0.63	3.71

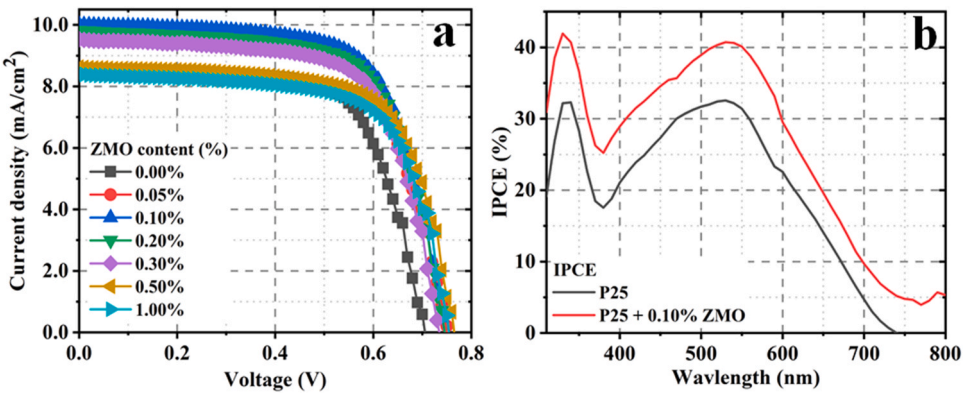

Fig. 7. (a) J-V curves and (b) IPCE of DSSCs with different wt% of ZMO.

for the higher J_0 [6,30,31]. Cell parameters can provide information on the loss mechanism in these solar cells [30,35]. Thus, the cell parameters of DSSCs are determined analytically using method of Phang et al. [36], which is based on single diode model. The predicted five PV cell parameters are presented in Fig. 9**.** ZMO doped TiO_2 electrode shows a slightly increased photovoltage V_{oc} from 0.71 to 0.75 V (Table 2). The explanation of V_{oc} can be improved by engineering a more favorable equilibrium Fermi-level position in TiO_2 [12,37]. The J_{pH} value is increased from 8.6 $mAcm^{-2}$ (undoped TiO_2) to 10.05 $mAcm^{-2}$ for 0.1 wt% doping concentration of ZMO, because ZMO provide an easy path to mover the charge carriers. With further increase in ZMO content, the J_{pH} gradually decreases and finally the value of J_{pH} is reduced to 8.41 $mAcm^{-2}$ for the content of ZMO 1.0 wt%. For the higher content of ZMO, the charge generation is reduced. Thus, the J_{pH} get reduced. However, the value R_{sh} gradually decreases with the increase amount of ZMO. Thus, R_{sh} value was reduced from 2506.01 Ωcm^2 (for undoped TiO_2) to 1597.27 Ωcm^2 for doping content of 1.0 wt% ZMO. The reduction of the

Table 2
Determined cell parameters of the fabricated DSSCs.

	Jsc mA/cm^2	Voc V	FF	η (%)	Rsh Ohm-cm^2	Rs Ohm-cm^2	n	J0 A/cm^2
P25	8.58	0.71	0.68	4.12	2506.01	9.20	1.48	7.78E-11
P25 + 0.05 wt% ZMO	9.91	0.75	0.65	4.84	2342.41	9.11	1.95	3.33E-09
P25 + 0.1 wt% ZMO	10.04	0.75	0.68	5.09	1802.61	6.36	1.82	1.16E-09
P25 + 0.2 wt% ZMO	9.85	0.75	0.68	4.96	1301.90	6.20	1.79	8.86E-10
P25 + 0.3 wt% ZMO	9.58	0.73	0.68	4.77	970.04	7.49	1.44	2.26E-11
P25 + 0.5 wt% ZMO	9.04	0.74	0.67	4.51	1646.96	6.72	1.65	1.20E-10
P25 + 1.0 wt% ZMO	8.40	0.75	0.69	4.33	1597.27	5.66	1.89	1.55E-09
ZMO	0.032	0.38	0.02	0.00024	–	–	–	–

–: no measure.

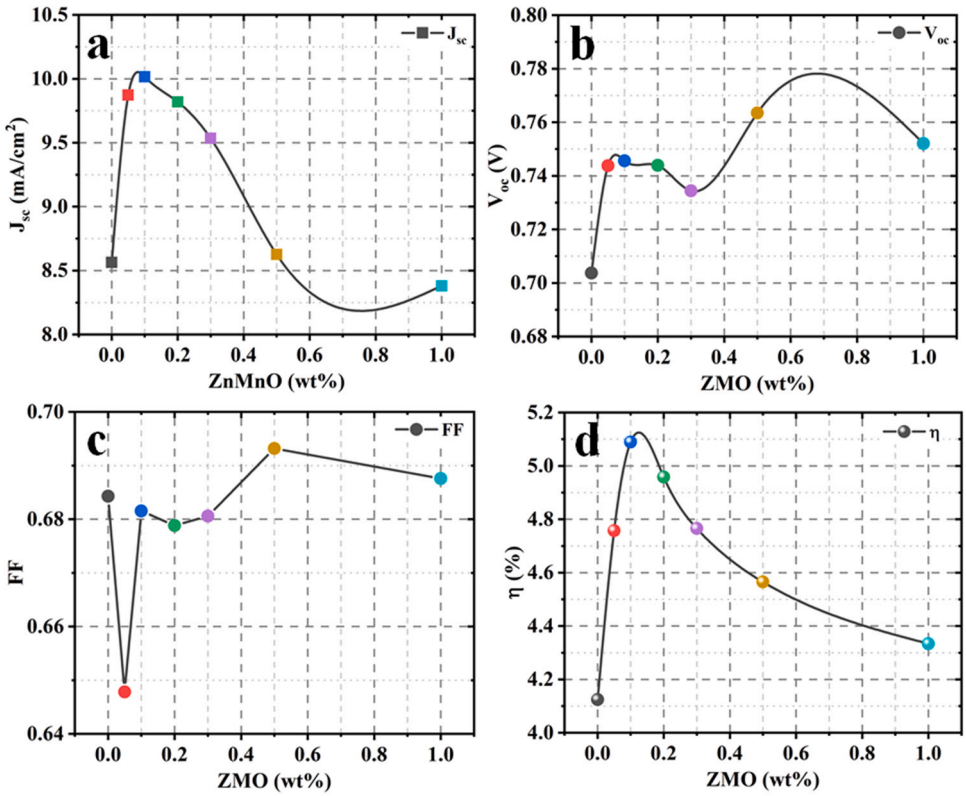

Fig. 8. Variation of performance parameters of DSSC for different content of ZMO.

R_{sh} value is due to insertion of the leakage (pores) path by ZMO. For the higher thickness of ZMO, the conductivity of the ZMO layer is reduced, thus the R_{sh} started to increase. The R_s was initially reduced from 9.20 Ωcm^2 to 5.66 Ωcm^2 for 0.20 wt% of ZMO. However, the value slightly increased for the doping content of 0.30 wt% (7.49 Ωcm^2) and 0.50 wt% (6.72 Ωcm^2). It again reduced to 5.66 Ωcm^2 for 1.0 wt% of ZMO. For a thin layer (0.1 wt% of ZMO), R_s is lowest because of insertion of the conducting path between TiO_2 and absorber. For the thicker layer (> 0.1 wt% of ZMO), the resistance of the path of the charge carriers is increased. Thus, R_s slightly increased for higher content of ZMO. Moreover, the value of n initially increased from 1.4812 (undoped TiO_2) to 1.9460 (0.05 wt%). With the further increase in the ZMO content, it decreases to 1.4447 for 0.3 wt%. The value of n again enhanced for further rise in the ZMO content. The obtained value of J_0 of TiO_2 DSSC was 7.78×10^{-11} Acm^{-2} which was initially increased to 3.33×10^{-9} Acm^{-2} for 0.05 wt% of ZMO. Further increase in the content of ZMO causes the reduction in the reverse saturation current density up to 0.3 wt% AZO. It attended a value of 2.26×10^{-11} Acm^{-2} for 0.3 wt%, however, J_0 again increased with the increase in the content of ZMO. Finally, it attended a value of 1.55×10^{-9} Acm^{-2} for the doping content of 1.0 wt% ZMO. These results revealed that 0.3 wt% of ZMO offer the lowest recombination in the devices [38]. Using these parameters, the composition of the composite photoanode can be adjusted and also the cell fabrication process can be improved for higher cell efficiency.

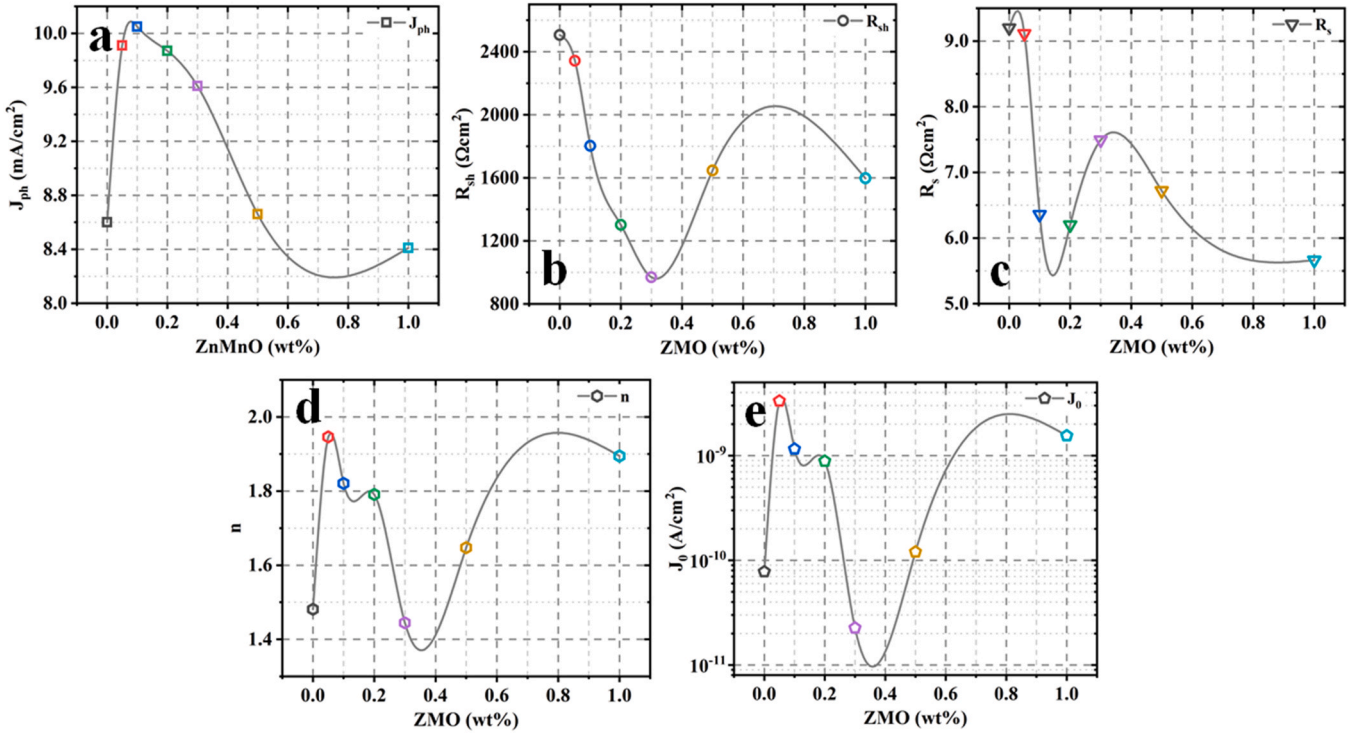

Fig. 9. Variation of PV cell parameters of DSSC for different content of ZMO.

4. Conclusion

ZMO nanoparticles were synthesized successfully under mild conditions. TEM spectrum confirms the formation of spherical structure with a particle size distribution of 20–40 nm, and the lattice size is about 0.26 nm, which is consistent with ZMO (211) crystal plane. EDAX analysis confirmed purity and presence of stoichiometric ratio of zinc, manganese and oxide in $ZnMn_2O_4$ nanoparticles. UV-Visible spectrum shows broader light-absorption by ZMO expanding from UV to visible region and the band gap was found to be 1.57 eV. Fabricated DSSC with 0.1% ZMO in the photoanode showed highest PCE of 5.08% which is nearly 23% higher than the cell with only P25 (PEC of 4.12%) at a film thickness of 24 μm. This was attributed to better dye loading and synergic contribution of the critical amount of ZMO particles within the photoanode which facilitated better charge separation and lower recombination. These eventually contributed to the increased short-circuit current and open-circuit voltage and hence improved PCE. Therefore, ZMO incorporated photoanode can be useful in future high-efficiency DSSCs.

Declaration of Competing Interest

We have no conflict of intrest.

Acknowledgment

This research was funded by the Deanship of Scientific Research at Princess Nourah bint Abdulrahman University through the Fast-track Research Funding Program.

Appendix A. Supporting information

Supplementary data associated with this article can be found in the online version at doi:10.1016/j.ijleo.2021.167976.

References

[1] Muhammad Norhaffis Mustafa, Yusran Sulaiman, Review on the effect of compact layers and light scattering layers on the enhancement of dye-sensitized solar cells, Sol. Energy 215 (2021) 26–43.
[2] Mohamed M. Abdel-Galeil, Rajesh Kumar, Atsunori Matsuda, Reda E. El-Shater, Investigation on influence of thickness variation effect of TiO2 film, spacer and counter electrode for improved dye-sensitized solar cells performance, Opt. Int. J. Light Electron Opt. 227 (2021), 166108.
[3] Yuqiang Liua, Yajuan Lia, Yiliang Wub, et al., High-Efficiency Silicon Heterojunction Solar Cells: Materials, Devices and Applications, Mater. Sci. Eng. R 142 (2020), 100579.
[4] Nick Vlachopoulos, Anders Hagfeldt, Iacopo Benesperi, Marina Freitag, Ghufran Hashmi, GuobinJia, Ruri Agung Wahyuono, Jonathan Plentzf, Benjamin Dietzek, New approaches in component design for dyesensitized solar cells, Sustain. Energy Fuels 5 (2021) 367.
[5] M. Gratzel, Recent advances in sensitized mesoscopic solar cells, Acc. Chem. Res. 42 (11) (2009) 1788–1798.
[6] (a) NerminKutlu, Investigation of electrical values of low-efficiency dye-sensitized solar cells (DSSCs), Energy 199 (2020), 117222;
(b) B.O. Regan, M. Gräzel, A low-cost, high-efficiency solar cell based on dye-sensitized colloidal TiO2 films, Nature 353 (1991) 737–117740.
[7] A. Hagfeldt, M. Gräzel, Light-induced redox reactions in nanocrystalline systems, Chem. Rev. 95 (1995) 49–68.
[8] Umer Mehmood, S.H.A. Ahmad, Amir Al-Ahmed, Abbas Saeed Hakeem, H. Dafalla, A. Laref, Synthesis and characterization of cerium oxide impregnated titanium oxide photoanodes for efficient dye-sensitized solar cells, IEEE J. Photovolt. 10 (2020) 1365–1370.
[9] Hani Sayahi, Kioumars Aghapoor, Farshid Mohsenzadeh, Mina MohebiMorad, Hossein Reza Darabi, TiO2 nanorods integrated with titania nanoparticles: large specific surface area 1D nanostructures for improved efficiency of dye-sensitized solar cells (DSSCs), Sol. Energy 215 (2021) 311–320.
[10] Nguyen Thi Quynh Hoa, Van-Duong Dao, Ho-Suk Choi, Facile one-pot synthesis of hierarchical TiO2 nanourchins for highly efficient dye-sensitized solar cells, J. Electrochem. Soc. 161 (12) (2014) X21. -X21.
[11] Van-Duong Dao, Liudmila L. Larina, Ho-Suk Choi, Plasma reduction of nanostructured TiO2 electrode to improve photovoltaic efficiency of dye-sensitized solar cells, J. Electrochem. Soc. 161 (2014) 161 H896.
[12] Ibrahim M.A.Mohamed Van-Duong Dao, Ahmed S. Yasin, Hamouda M.Mousaa Hend Omar Mohamed, Ho-Suk Choi, Mohamed K. Hassan, Nasser A.M. Barakat, Nitrogen-doped&SnO2-incoportaed TiO2 nanofibers as novel and effective photoanode for enhanced efficiency dye-sensitized solar cells, Chem. Eng. J. 304 (2016) 48–60.
[13] K. Eguchi, H. Koga, K. Sekizawa, Nb2O5-based composite electrodes for dye-sensitized solar cells, J. Ceram. Soc. Jpn. 108 (2000) 1067–1071.
[14] X. Feng, K. Shankar, M. Paulose, C.A. Grimes, Tantalum-doped titanium dioxide nanowire arrays for dye-sensitized solar cells with high open-circuit voltage, AngewChemie 121 (2009) 8239–8242.
[15] Yandong Duan, Nianqing Fu, Qiuping Liu, Yanyan Fang, Xiaowen Zhou, Jingbo Zhang, Yuan Lin, Sn-doped TiO_2 photoanode for dye-sensitized solar cells, J. Phys. Chem. C 116 (16) (2012) 8888–8893.
[16] W. Ahmad, U. Mehmood, A. Al-Ahmed, F.A. Al-Sulaiman, M.Z. Aslam, M.S. Kamal, Synthesis of zinc oxide/titanium dioxide (ZnO/TiO_2) nanocomposites by wet incipient wetness impregnation method and preparation of ZnO/TiO_2 paste using poly(vinylpyrrolidone) for efficient dye-sensitized solar cells, Electro Acta 222 (2016) 473–480.
[17] U. Mehmood, Z. Malaibari, F.A. Rabani, A.U. Rehman, S.H.A. Ahmad, M.A. Atieh, Photovoltaic improvement and charge recombination reduction by aluminum oxide impregnated MWCNTs/TiO2based photoanode for dye-sensitized solar cells, Electrochim. Acta 203 (2016) 162–170.
[18] M. Younas, M.A. Gondal, M.A. Dastageer, U. Baig, Fabrication of cost effective and efficient dye sensitized solar cells with WO3-TiO2 nanocomposites as photoanode and MWCNT as Pt-free counter electrode, Ceram. Int. 45 (2019) 936–947.
[19] L. Zhao, X. Li, J. Zhao, Fabrication, characterization and photocatalytic activity of cubic-like ZnMn2O4, Appl. Surf. Sci. 268 (2013) 274e277.
[20] F.M. Courtel, Y. Abu-Lebdeh, I.J. Davidson, ZnMn2O4 nanoparticles synthesized by a hydrothermal method as an anode material for Li-ion batteries, ElectrochimicaActa 71 (2012) 123e127.
[21] X.F. Chen, L. Qie, L.L. Zhang, W.X. Zhang, Y.H. Huang, Self-templated synthesis of hollow porous submicron ZnMn2O4 sphere as anode for lithium-ion batteries, J. Alloy. Compd. 559 (2013) 5e10.

[22] Pan Zhang, Xinyong Li, Qidong Zhao, Shaomin Liu, Synthesis and optical property of one dimensional spinel ZnMn2O4 nanorods, Zhang et al, Nanoscale Res. Lett. 6 (2011) 323.
[23] Fabrice M. Courtel, Hugues Duncan, Yaser Abu-Lebdeh, Isobel J. Davidson, High capacity anode materials for Li-ion batteries based on spinel metal oxides AMn2O4 (A = Co, Ni, and Zn), J. Mater. Chem. 21 (2011) 10206–10218.
[24] Chih-Hung Tsai, Chia-Ming Lin, Yen-Cheng Liu, Increasing the efficiency of dye-sensitized solar cells by adding nickel oxide nanoparticles to titanium dioxide working electrodes, Coatings 10 (2020) 195.
[25] S. Kiran, S.K. Naveen Kumar, Preparation and thickness optimization of TiO_2/Nb_2O_5 photoanode for dye sensitized solar cells, Mater. Today Proc. 5 (2018) 10797–10804.
[26] Hadja Fatima Mehnane, Changlei Wang, Kiran Kumar Kondamareddy, Wenjing Yu, Weiwei Sun, Haimin Liu, Sihang Bai, Wei Liu, Shishang Guo, Xing-Zhong Zhao, Hydrothermal synthesis of TiO_2nanoparticles doped with trace amounts of strontium, and their application as working electrodes for dye sensitized solar cells: tunable electrical properties & enhanced photo-conversion performance, RSC Adv. 7 (2017) 2358–2364.
[27] T. Raguram, K.S. Rajni, Influence of boron doping on the structural, spectral, optical and morphological properties of TiO2 nanoparticles synthesized by sol–gel technique for DSSC applications, Mater. Today Proc. 33 (2020) 2110–2115.
[28] Hongna Zhang, Benlin He, Qunwei Tang, Enhanced light harvesting of TiO2/La0.95Tb0.05PO4 photoanodes for dye-sensitized solar cells, Mater. Chem. Phys. 173 (2016) 340–346.
[29] Rama Krishna Chava, Misook Kang, Improving the photovoltaic conversion efficiency of ZnO based dye sensitized solar cells by indium doping, J. Alloy. Compd. 692 (2017) 67e76.
[30] Suyitno Zainal Arifin, Syamsul Suyitno, Hadi, Bayu Sutanto, Improved performance of dye-sensitized solar cells with TiO2 nanoparticles/Zn-doped TiO2 hollow fiber photoanodes, Energies 11 (2018) 2922, https://doi.org/10.3390/en11112922.
[31] D. Wongratanaphisan, K. Kaewyai, S. Choopuna, A. Gardchareon, P. Ruankham, S. Phadungdhitidhada, CuO-Cu2O nanocomposite layer for light-harvesting enhancement in ZnO dye-sensitized solar cells, Appl. Surf. Sci. 474 (2019) 85–90.
[32] Seval Aksoy, Ozgur Polat, Kamuran Gorgun, Yasemin Caglar, Mujdat Caglar, Li doped ZnO based DSSC: characterization and preparation of nanopowdersand electrical performance of its DSSC, Phys. E Low Dimens. Syst. Nanostruct. 121 (2020) 114–127.
[33] Mian-En Yeoh, Kah-Yoong Chan, Dietmar Knipp, Simplified electrical modeling for dye sensitized solar cells: Influences of the blocking layer and chenodeoxycholic acid additive, Solid State Electron. 180 (2021), 107983.
[34] F. Khan, B.D. Rezgui, J.H. Kim, Analysis of PV cell parameters of solution processed Cu-doped nickel oxide hole transporting layer-besed organic-inorganic perovskite solar cell, Sol. Energy 209 (2020) 226–234.
[35] F. Khan, S.H. Baek, J.H. Kim, Intensity dependency of photovoltaic cell parameters under high illumination conditions: an analysis, Appl. Energy 133 (2014) 356–362.
[36] J.C.H. Phang, D.S.H. Chan, J.R. Phillips, Accurate analytical method for the extraction of solar cell model parameters, Electron Lett. 20 (1984) 406–408.
[37] Van-Duong Dao, Seong-Hoon Kim, Ho-Suk Choi, Jae-Ha Kim, Han-Oh Park, Joong-Kee Lee, Efficiency enhancement of dye-sensitized solar cell using Pt hollow sphere counter electrode, J. Phys. Chem. C 115 (2011) 25529–25534.
[38] Van-Duong Dao, Comment on "Energy storage via polyvinylidene fluoride dielectric on the counter electrode of dye-sensitized solar cells, J. Power Sources 337 (2017) 125–129.